

Quasi-elastic neutrino charged-current scattering off medium-heavy nuclei: ^{40}Ca and ^{40}Ar

A. V. Butkevich

*Institute for Nuclear Research, Russian Academy of Sciences,
60th October Anniversary Prosp. 7A, Moscow 117312, Russia*

(Dated: November 29, 2018)

The charged-current quasi-elastic scattering of muon neutrinos on calcium and argon targets is calculated for neutrino energy up to 2.8 GeV. The calculations are done within the framework of the relativistic distorted-wave impulse approximation, which was earlier successfully applied to describe electron-nucleus data. The model is first tested against experimental data for electron scattering off calcium and then it is applied to calculate (anti)neutrino cross sections on ^{40}Ca and ^{40}Ar . We show that reduced exclusive cross sections for neutrino and electron scattering are similar. A significant nuclear model dependence of both inclusive and total cross sections for energy about 1 GeV was found. From the comparison of the (anti)neutrino differential and total cross sections per (proton)neutron, calculated for the carbon, oxygen, and argon targets it is evident that the cross sections decrease slowly with the mass-number of the target due to nuclear effects.

PACS numbers: 25.30.-c, 25.30.Bf, 25.30.Pt, 13.15.+g

I. INTRODUCTION

The investigation of neutrino oscillations and the precision measurements of neutrino oscillation parameters brought extremely intense neutrino beams. In this situation, statistical uncertainties are negligible compared to those systematic uncertainties in the neutrino flux, neutrino-nucleus cross sections, and detector effects on both neutrino events selection and neutrino energy reconstruction. Thus, the discovery and study of neutrino oscillations have renewed interest in neutrino-nucleus interactions. The high intensity neutrino beams allow to study these processes with unprecedented details.

In order to study neutrino oscillation effects in accelerator-based experiments, the neu-

trino beams cover the energy range from a few hundred MeV to several GeV. In this energy range, the dominant contribution to the neutrino-nucleus cross section comes from the charged-current quasielastic (CCQE) reaction and resonance production processes. The CCQE is the simplest interaction that represents a two-particle scattering process with single final-state proton and it may form a two track events sample. In this process the neutrino energy may be estimated using kinematic or calorimetric reconstruction.

The criteria used to select CCQE events is strongly influenced by both the target material and the detector technology. In fully active, fine-grained detectors with good resolution, selection techniques that rely on the identification of a single final state proton and lepton can be applied. One option for these detector designs is to make their active elements as water [1], scintillator [2–5] bars or drift chambers [6] formed in to detector planes. A continuous series of these planes forms a region that serves as both primary target and tracking detector.

Another option for fully active and fine-grained detectors is liquid argon time projection chamber (LAr TPC) [7, 8] which offers a relatively good particle identification. The high spatial resolution and energy measurement down to the MeV scale provides information for low and high energy particles. This information allows reduced background for the events of interest and potentially improved cross section measurements. The LAr TPC detectors are well-suited for long baseline ν_e appearance physics because of their high efficiency for ν_e ‘signal’ events and low background from ν_μ events [9]. Therefore, there is a growing interest in measuring neutrino cross sections on argon.

Unfortunately, the cross section data for lepton scattering on argon in relevant energy range are rather scarce. There are only experimental data for inclusive 700-MeV electron scattering off ^{40}Ar [10]. On the other hand the structures of ^{40}Ca and ^{40}Ar nuclei are almost identical and for calcium precise measurements have been performed and are described below.

High resolution exclusive ($e, e'p$) experiments, where a proton is emitted with a direct knockout mechanism on ^{40}Ca and ^{48}Ca were carried out at Tokyo [11, 12], Saclay [13], and NIKHEF [14–16]. Specific quantum numbers and spectroscopic factors have been assigned to the peaks in the observed energy spectrum by studying the missing energy and momentum dependence of experimental cross sections. The data analysis of this processes was performed within the theoretical framework of the nonrelativistic distorted-wave impulse approximation

(DWIA) [17, 18] and relativistic DWIA (RDWIA) [19] in Refs. [14–16, 20–25]. There, the RDWIA approach was able to describe with high degree of accuracy the experimental shape of the outgoing particle momentum distributions. In order to reproduce experimental cross sections, normalization of the bound-state wave functions were fitted to the data and identified with the spectroscopic factors.

Inclusive (e, e') cross sections of the electron scattering on calcium were measured with good accuracy in a series of experiments [26–30]. In Refs. [28, 30] the transverse and longitudinal nuclear response functions were extracted. The comparison of different models with the data is described in Refs [31, 32].

In this work we compute the exclusive, inclusive and total cross sections for the CCQE neutrino scattering from ^{40}Ca and ^{40}Ar using the RDWIA model. The calculations of the inclusive cross sections are performed with our approach, which includes the final state interaction (FSI) effects in the presence of short-range nucleon-nucleon (NN) correlations in the ground state [33]. This approach was successfully applied in Refs. [34–37]. First we compare our model in describing $^{40}\text{Ca}(e, e')^{39}\text{K}$ and $^{40}\text{Ca}(e, e')$ data. Then we apply it to the calculation of the CCQE cross sections for the neutrino scattering on ^{40}Ca and ^{40}Ar nuclei.

The goals of this work are the following: (a) calculation of the RDWIA CCQE $\nu^{40}\text{Ar}$ cross sections, (b) comparison of the total cross sections, scaled with the number of (proton)neutrons in the target for (anti)neutrino scattering on the carbon, oxygen, and argon targets, and (c) investigation of nuclear effects on these cross sections.

The paper is organized as follows. In Sec. II we present briefly the formalism for the CCQE scattering process and basic aspects of the model used for the calculation. The results are presented and discussed in Sec. III. Our conclusions are summarized in Sec. IV.

II. FORMALISM OF QUASI-ELASTIC SCATTERING AND RDWIA

In this section we consider shortly the formalism used to describe electron and neutrino quasi-elastic exclusive

$$l(k_i) + A(p_A) \rightarrow l'(k_f) + N(p_x) + B(p_B), \quad (1)$$

and inclusive

$$l(k_i) + A(p_A) \rightarrow l'(k_f) + X \quad (2)$$

scattering off nuclei in the one-photon (W-boson) exchange approximation. Here l labels the incident lepton [electron or muon (anti)neutrino], and l' represents the scattered lepton (electron or muon), $k_i = (\varepsilon_i, \mathbf{k}_i)$ and $k_f = (\varepsilon_f, \mathbf{k}_f)$ are the initial and final lepton momenta, $p_A = (\varepsilon_A, \mathbf{p}_A)$, and $p_B = (\varepsilon_B, \mathbf{p}_B)$ are the initial and final target momenta, $p_x = (\varepsilon_x, \mathbf{p}_x)$ is the ejectile nucleon momentum, $q = (\omega, \mathbf{q})$ is the momentum transfer carried by the virtual photon (W-boson), and $Q^2 = -q^2 = \mathbf{q}^2 - \omega^2$ is the photon (W-boson) virtuality.

A. CCQE neutrino-nucleus cross sections

In the laboratory frame, the differential cross section for the exclusive electron (σ^{el}) and (anti)neutrino CCQE (σ^{cc}) scattering, in which only a single discrete state or narrow resonance of the target is excited, can be written as

$$\frac{d^5\sigma^{el}}{d\varepsilon_f d\Omega_f d\Omega_x} = R \frac{|\mathbf{p}_x| \varepsilon_x \varepsilon_f \alpha^2}{(2\pi)^3 \varepsilon_i Q^4} L_{\mu\nu}^{(el)} W^{\mu\nu(el)} \quad (3a)$$

$$\frac{d^5\sigma^{cc}}{d\varepsilon_f d\Omega_f d\Omega_x} = R \frac{|\mathbf{p}_x| \varepsilon_x |\mathbf{k}_f| G^2 \cos^2 \theta_c}{(2\pi)^5 \varepsilon_i 2} L_{\mu\nu}^{(cc)} W^{\mu\nu(cc)}, \quad (3b)$$

where R is a recoil factor, Ω_f is the solid angle for the lepton momentum, Ω_x is the solid angle for the ejectile nucleon momentum, $\alpha \simeq 1/137$ is the fine-structure constant, $G \simeq 1.16639 \times 10^{-11} \text{ MeV}^{-2}$ is the Fermi constant, θ_C is the Cabbibo angle ($\cos \theta_C \approx 0.9749$), $L_{\mu\nu}$ is the lepton tensor and $W_{\mu\nu}^{(el)}$ and $W_{\mu\nu}^{(cc)}$ are the electromagnetic and weak CC nuclear tensors, respectively. The energy ε_x is the solution to the equation

$$\varepsilon_x + \varepsilon_B - m_A - \omega = 0, \quad (4)$$

where $\varepsilon_B = \sqrt{m_B^2 + \mathbf{p}_B^2}$, $\mathbf{p}_B = \mathbf{q} - \mathbf{p}_x$, $\mathbf{p}_x = \sqrt{\varepsilon_x^2 - m^2}$, and m_A , m_B , and m are masses of the target, recoil nucleus and nucleon, respectively. The missing momentum p_m and missing energy ε_m are defined by

$$\mathbf{p}_m = \mathbf{p}_x - \mathbf{q} \quad (5a)$$

$$\varepsilon_m = m + m_B - m_A. \quad (5b)$$

The leptonic tensor is separated into a symmetrical and an anti-symmetrical components that are written as in Ref. [33]. For electron scattering at energies considered in this work, a

simple and accurate enough effective momentum approximation [23, 38] to include the effects of Coulomb distorted wave functions is used. All information about the nuclear structure and FSI effects is contained in the electromagnetic and weak CC hadronic tensors, $W_{\mu\nu}^{(el)}$ and $W_{\mu\nu}^{(cc)}$, which are given by the bilinear products of the transition matrix elements of the nuclear electromagnetic or CC operator $J_\mu^{(el)(cc)}$ between the initial nucleus state $|A\rangle$ and the final state $|B_f\rangle$ as

$$W_{\mu\nu}^{(el)(cc)} = \sum_f \langle B_f, p_x | J_\mu^{(el)(cc)} | A \rangle \langle A | J_\nu^{(el)(cc)\dagger} | B_f, p_x \rangle, \quad (6)$$

where the sum is taken over undetected states.

The experimental data of the $(e, e'p)$ reaction are usually presented in terms of the reduced cross section

$$\sigma_{red} = \frac{d^5\sigma}{d\varepsilon_f d\Omega_f d\Omega_x} / K^{(el)(cc)} \sigma_{lN}, \quad (7)$$

where $K^{el} = Rp_x \varepsilon_x / (2\pi)^3$ and $K^{cc} = Rp_x \varepsilon_x / (2\pi)^5$ are phase-space factors for electron and neutrino scattering and σ_{lN} is the corresponding elementary cross section for the lepton scattering from the moving free nucleon. The reduced cross section is an interesting quantity that can be regarded as the nucleon momentum distribution modified by FSI. It was shown in Refs. [33, 35] that reduced cross sections for (anti)neutrino scattering off carbon and oxygen are similar to the electron scattering apart from small differences at low beam energy due to effects of Coulomb distortion of the incoming electron wave function.

B. Models

We describe the lepton-nuclear scattering in the impulse approximation (IA), assuming that the incoming lepton interacts with only one nucleon of the target, which is subsequently emitted, while the remaining $(A-1)$ nucleons in the target are spectators. When the nuclear current is written as a sum of single-nucleon currents, the nuclear matrix element in Eq.(6) can write as

$$\langle p, B | J^\mu | A \rangle = \int d^3r \exp(it \cdot \mathbf{r}) \bar{\Psi}^{(-)}(\mathbf{p}, \mathbf{r}) \Gamma^\mu \Phi(\mathbf{r}), \quad (8)$$

where Γ^μ is the vertex function, $\mathbf{t} = \varepsilon_B \mathbf{q} / W$ is the recoil-corrected momentum transfer, $W = \sqrt{(m_A + \omega)^2 - \mathbf{q}^2}$ is the invariant mass, Φ and $\Psi^{(-)}$ are the relativistic bound-state and outgoing wave functions.

For electron scattering, we use the CC2 electromagnetic vertex function for a free nucleon [40]

$$\Gamma^\mu = F_V^{(el)}(Q^2)\gamma^\mu + i\sigma^{\mu\nu}\frac{q_\nu}{2m}F_M^{(el)}(Q^2), \quad (9)$$

where $\sigma^{\mu\nu} = i[\gamma^\mu, \gamma^\nu]/2$, $F_V^{(el)}$ and $F_M^{(el)}$ are the Dirac and Pauli nucleon form factors. The single-nucleon charged current has $V-A$ structure $J^{\mu(cc)} = J_V^\mu + J_A^\mu$. For a free-nucleon vertex function $\Gamma^{\mu(cc)} = \Gamma_V^\mu + \Gamma_A^\mu$ we use the CC2 vector current vertex function

$$\Gamma_V^\mu = F_V(Q^2)\gamma^\mu + i\sigma^{\mu\nu}\frac{q_\nu}{2m}F_M(Q^2) \quad (10)$$

and the axial current vertex function

$$\Gamma_A^\mu = F_A(Q^2)\gamma^\mu\gamma_5 + F_P(Q^2)q^\mu\gamma_5. \quad (11)$$

The weak vector form factors F_V and F_M are related to the corresponding electromagnetic form factors $F_V^{(el)}$ and $F_M^{(el)}$ for protons and neutrons by the hypothesis of the conserved vector current. We use the approximation of Ref. [39] for the Dirac and Pauli nucleon form factors. Because the bound nucleons are the off-shell we employ the de Forest prescription [40] and Coulomb gauge for the off-shell vector current vertex Γ_V^μ . The vector-axial F_A and pseudoscalar F_P form factors are parametrized using a dipole approximation:

$$F_A(Q^2) = \frac{F_A(0)}{(1 + Q^2/M_A^2)^2}, \quad F_P(Q^2) = \frac{2mF_A(Q^2)}{m_\pi^2 + Q^2}, \quad (12)$$

where $F_A(0) = 1.267$, M_A is the axial mass, which controls Q^2 -dependence of $F_A(Q^2)$, and m_π is the pion mass.

In RDWIA calculations the independent particle shell model (IPSM) is assumed for the nuclear structure. In Eq.(8) the relativistic bound-state wave function for nucleons Φ are four-spinors that are obtained as the self-consistent (Hartree–Bogolioubov) solutions of a Dirac equation, derived within a relativistic mean-field approach, from a Lagrangian containing σ , ω , and ρ mesons [41–43]. We use the nucleon bound-state functions calculated by the TIMORA code [43] with the normalization factors $S(\alpha)$ relative to full occupancy of the IPSM orbitals of ^{40}Ca and ^{40}Ar . The source of the reduction of the $(e, e'p)$ spectroscopic factors with respect to the mean field values are the short-range and tensor correlations, which arise from the characteristics of the bare nucleon-nucleon interaction and long-range correlations related to the coupling between single-particle motion and collective surface vibrations.

For an outgoing nucleon, the simplest choice is to use the plane-wave function Ψ , assuming that there is no interaction between the ejected nucleon N and the residual nucleus B . In this plane-wave impulse approximation (PWIA) the exclusive cross section is factorized into the product of the phase-space factor K , elementary off-shell lepton-nucleon scattering cross section, and the hole spectral function. Thus, in the PWIA the reduced cross section can be interpreted as the momentum distribution of the emitted nucleon when it was inside the nucleus. For more realistic description, FSI effects should be taking into account. In the RDWIA the distorted wave function Ψ is evaluated as a solution of the Dirac equation containing a phenomenological relativistic optical potential. This potential consists of a real part, which describes the rescattering of the ejected nucleon and an imaginary part which accounts for its absorption into unobserved channels.

Using the direct Pauli reduction method [24], the system of two coupled first-order Dirac equations can be reduced to a single second-order Schrödinger-like equation for the upper component of the Dirac wave function Ψ . This equation contains equivalent nonrelativistic central and spin-orbit potentials which are functions of the relativistic, energy dependent, scalar, and vector optical potentials. We use the LEA program [44] for the numerical calculation of the distorted wave functions with the EDAD1 parametrization [45] of the relativistic optical potential for calcium. This code was successfully tested against $A(e, e'p)$ data for electron scattering off ^{12}C and ^{16}O [46, 47] and we adopted this program for neutrino reaction [33].

A complex optical potential with a nonzero imaginary part generally produces an absorption of the flux. For the exclusive $A(l, l'N)$ channel this reflects the coupling between different open reaction channels. However, for the inclusive reaction, the total flux must be conserved. In Refs. [48, 49], it was shown that the inclusive CCQE neutrino cross section of the exclusive channel $A(l, l'N)$ is calculated with only the real part of the optical potential is almost identical when calculated via the Green's function approach [48], in which the FSI effects on inclusive reaction $A(l, l'X)$ are treated by means of a complex potential, and the total flux is conserved. We calculate the inclusive and total cross sections with the EDAD1 relativistic optical potential in which only the real part is included. The inclusive cross sections with the FSI effects in the presence of the short-range NN correlations are calculated using the method proposed in Ref. [33]. In this approach the contribution of the NN correlated pairs is evaluated in the PWIA. The FSI effects for the high-momentum component

are estimated by scaling the PWIA cross section with the $\Lambda(\varepsilon_f, \Omega_f)$ function determined in Ref. [33].

III. RESULTS AND ANALYSIS

A. Electron scattering

In this work the IPSM is assumed for the ^{40}Ca and ^{40}Ar nuclear structures. The model space for $^{40}\text{Ca}(l, l'N)$ consists of $1s_{1/2}$, $1p_{3/2}$, $1p_{1/2}$, $1d_{5/2}$, $2s_{1/2}$ and $1d_{3/2}$ nucleon-hole states in ^{39}K and ^{39}Ca nuclei. The model space for $^{40}\text{Ar}(l, l'N)$ consists of $1s_{1/2}$, $1p_{3/2}$, $1p_{1/2}$, $1d_{5/2}$, $2s_{1/2}$ and $1d_{3/2}$ nucleon-hole states in ^{39}Cl , and $1s_{1/2}$, $1p_{3/2}$, $1p_{1/2}$, $1d_{5/2}$, $2s_{1/2}$, $1d_{3/2}$ and $1f_{7/2}$ nucleon-hole states in ^{39}Ar . All states are regarded as a discrete states even though their spreading widths are actually appreciable.

First we show the performances of the LEA program in describing of experimental data for the $^{40}\text{Ca}(e, e'p)$ reaction measured at NIKHEF in (\mathbf{q}, ω) constant kinematics [14, 16]. The comparison with the experimental reduced cross sections is displayed in Fig.1. We have considered cross sections for the removal of the proton from the $1d_{3/2}$ shell, for transition to the $1/2^+$ excited state of the ^{39}K nucleus at the excitation energy of $E_x=2.522$ MeV, and for the transitions to the $5/2^+$ excited states at $E_x=5.258$ MeV and $E_x=6.328$ MeV, obtained by knocking out protons from the $2s_{1/2}$ and $1d_{5/2}$ orbitals, correspondingly. It should be noted that positive (negative) values of p_m refer to situations where the angle between the outgoing proton momentum \mathbf{p}_m and the incident electron \mathbf{k}_i is larger (smaller) than the angle between \mathbf{q} and \mathbf{k}_i .

The missing momentum distribution calculated in the RDWIA approach is shown in Fig.1 with NIKHEF data [14] and provide a good description of the shape of the measured distribution. Normalization factors have been applied to reproduce the magnitude of the measured reduced cross sections. The factors of 0.68, 0.51, 0.11, and 0.13 for the transition to the $3/2^+$, $1/2^+$ ($E_x=2.522$ MeV), $5/2^+$ ($E_x=5.258$ MeV), and $5/2^+$ ($E_x=6.328$ MeV) states, correspondingly are almost identical to those obtained in the data analysis of Refs. [16, 25]. Neutrino and antineutrino reduced cross sections of $^{40}\text{Ca}(\nu, \mu^- p)^{39}\text{Ca}$ and $^{40}\text{Ca}(\bar{\nu}, \mu^+ n)^{39}\text{K}$ reactions also shown are in Fig.1. They were calculated with the same reduced factors as electron cross sections. There is an overall good agreement between calculated cross sections,

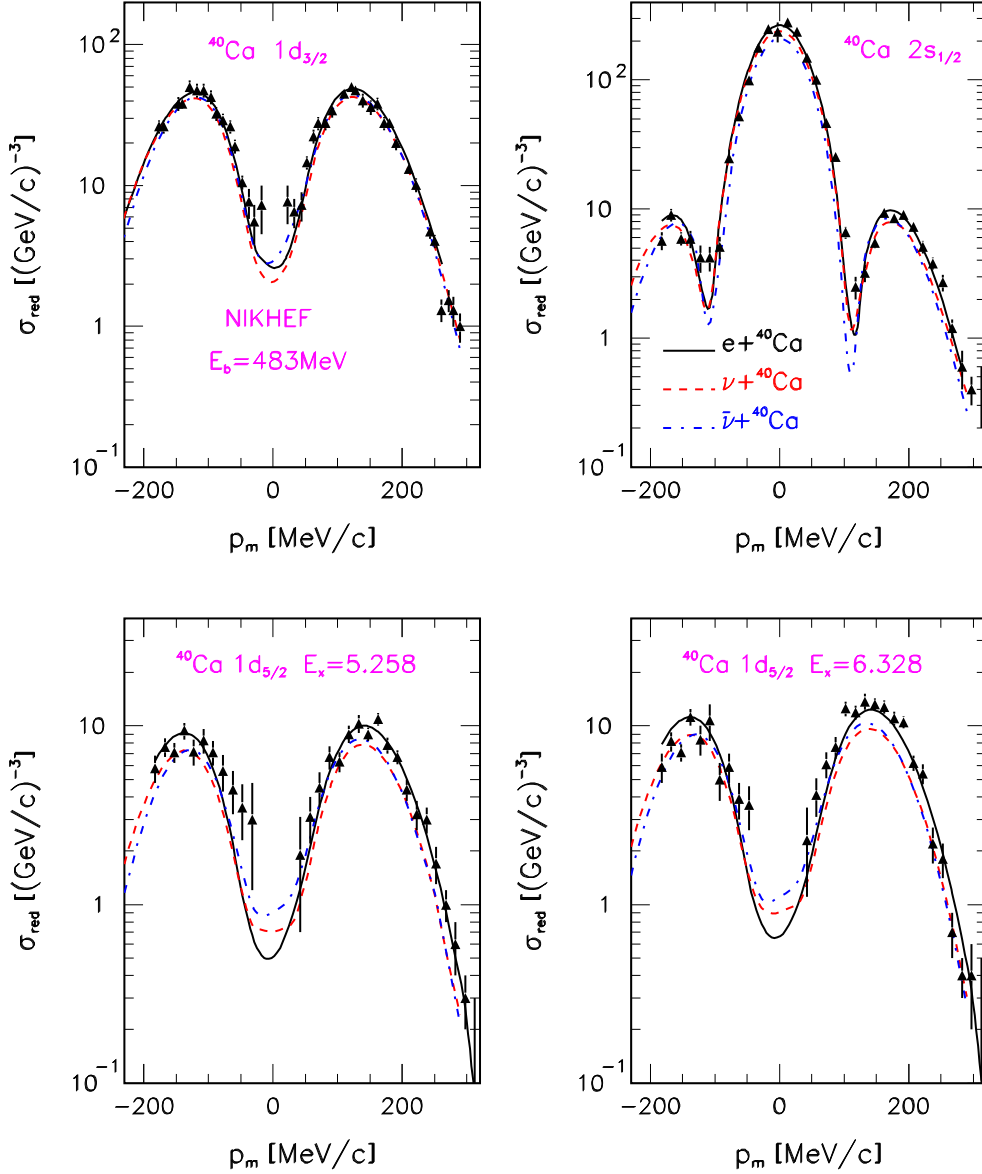


FIG. 1: (Color online) Comparison of the RDWIA calculations for electron (solid line), neutrino (dashed line), and antineutrino (dashed-dotted line) reduced cross sections for the removal of nucleons from $1d_{3/2}$, $2s_{1/2}$, and $1d_{5/2}$ shells of ^{40}Ca with NIKHEF data [16]. We show the results obtained in (\mathbf{q}, ω) constant kinematics for electron beam energy $E_{beam}=483.2$ MeV, the outgoing proton kinetic energy $T_p=100$ MeV, and $\mathbf{q}=450$ $(\text{MeV}/c)^2$. The cross sections are presented as functions of missing momentum p_m for the transition to the $3/2^+$ ground state, $1/2^+$ ($E_x=2.522$ MeV), and $5/2^+$ ($E_x=5.258, 6.328$ MeV) excited states of ^{39}K and ^{39}Ca .

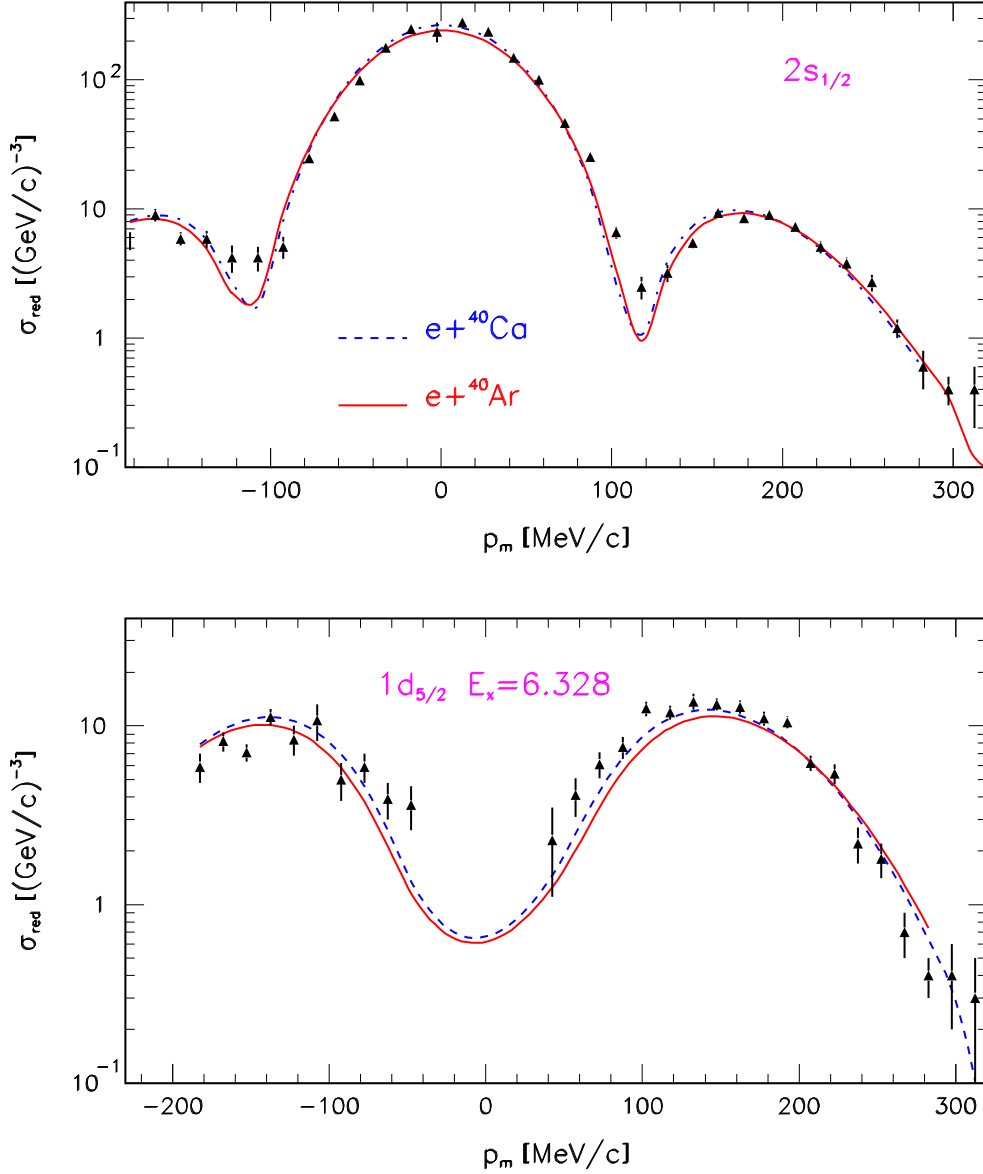


FIG. 2: (Color online) Reduced cross sections of the $^{40}\text{Ar}(e, e'p)$ (solid line) and $^{40}\text{Ca}(e, e'p)$ (dashed line) reactions as functions of missing momentum p_m for the transitions to the $1/2^+$ ($E_x=2.522$ MeV) and $5/2^+$ ($E_x=6.328$ MeV) excited states in ^{39}Cl and ^{39}K . For comparison the data for the $^{40}\text{Ca}(e, e'p)$ reaction are shown from Ref. [16].

but the values of the electron cross sections at the maximum is systematically higher than those for (anti)neutrino. This can be attributed to Coulomb distortion upon the incident electron wave function. The small difference between neutrino and antineutrino is due to difference in the FSI of the proton and neutron with the residual nucleus.

TABLE I: Proton and neutron binding energies (E_b) and the occupancies for ^{40}Ca .

| Orbital | E_b (MeV) | | S |
|------------|-------------|------|------|
| | p | n | |
| $1s_{1/2}$ | 57.4 | 64.3 | 1 |
| $1p_{3/2}$ | 36.5 | 43.5 | 0.95 |
| $1p_{1/2}$ | 31.6 | 38.7 | 0.95 |
| $1d_{5/2}$ | 15.4 | 22.6 | 0.80 |
| $2s_{1/2}$ | 10.9 | 18.1 | 0.85 |
| $1d_{3/2}$ | 8.3 | 15.6 | 0.82 |

In Fig.2 we compare our results for the $^{40}\text{Ar}(e, e'p)$ reaction for transitions to the $1/2^+$ ($E_x=2.522$ MeV) and $5/2^+$ ($E_x=6.328$ MeV) excited states of ^{39}K with the $^{40}\text{Ca}(e, e'p)$ data. Also in this case, the results are multiplied by the same normalization factors (0.51 and 0.13) as for the $^{40}\text{Ca}(e, e'p)$ reduced cross sections. In this figure for comparison shown are the calculated reduced cross-section for the $^{40}\text{Ca}(e, e'p)$ reaction. The cross sections for the removal protons from the $1/2^+$ and $5/2^+$ shells of ^{40}Ca and ^{40}Ar as functions of p_m are very similar, but at the maximum the values of the cross sections for ^{40}Ar are systematically lower (less than 12%) than for ^{40}Ca .

Mean values of the proton and neutron binding energies and occupancies of shells that used in this work are listed in Table I for ^{40}Ca and in Table II for ^{40}Ar . The values of the proton and neutron binding energies for the $1d_{3/2}$, $2s_{1/2}$, and $1d_{5/2}$ shells, as well as those for neutron for the $1f_{7/2}$ orbital in ^{40}Ar were taken from Ref. [50]. For the $1p_{3/2}$, $1p_{1/2}$, and $1s_{1/2}$ deeply bound orbitals proton and neutron binding energies were estimated in Refs. [51, 52]. In Ref. [16] the $2p_{3/2}$, $1f_{7/2}$, $1d_{3/2}$, $2s_{1/2}$, and $1d_{5/2}$ strengths were obtained as a sum of the strengths arising from the discrete transitions and strengths which are observed in the continuum at higher excitation energies. In Table I occupancy of the $1d_{3/2}$, $2s_{1/2}$, and $1d_{5/2}$ orbitals from Ref. [16] are shown. The occupancy of the $1p_{3/2}$ and $1p_{1/2}$ shells were estimated from the $^{40}\text{Ca}(e, e'p)$ data analysis in Ref. [13]. For the $1s_{1/2}$ shell we assume that occupancy is equal to 1.

Note, that in the IPSM the 20 protons and 20 neutrons of ^{40}Ca fill the shells up to the

TABLE II: Proton and neutron binding energies (E_b) and the occupancies for ^{40}Ar .

| Orbital | E_b (MeV) | | S | |
|------------|-------------|------|------|------|
| | p | n | p | n |
| $1s_{1/2}$ | 57.4 | 64.3 | 1 | 1 |
| $1p_{3/2}$ | 36.5 | 43.5 | 0.95 | 0.95 |
| $1p_{1/2}$ | 31.6 | 38.7 | 0.95 | 0.95 |
| $1d_{5/2}$ | 15.4 | 22.6 | 0.80 | 0.80 |
| $2s_{1/2}$ | 10.9 | 18.1 | 0.85 | 0.85 |
| $1d_{3/2}$ | 8.3 | 15.6 | 0.85 | 0.82 |
| $1f_{7/2}$ | | 9.87 | | 0.82 |

$1d_{3/2}$ orbital whereas the first empty orbital is the $1f_{7/2}$ orbital. Ground-state correlations manifest themselves by a depletion of the orbitals below and a filling the orbitals above Fermi level, i.e. nucleons from the $1d_{3/2}$ and $2s_{1/2}$ shells are promoted to the $1f_{7/2}$ and $2s_{1/2}$ orbitals. We include the observed $1f_{7/2}$ ($E_x=2.814$ MeV) and $2p_{3/2}$ ($E_x=3.019$ MeV) strength of 0.36 in the $2s_{1/2}$ shell because the observed missing-energy spectrum [16] of these orbitals strongly overlap. The rest of the $1f_{7/2}$ and $2p_{3/2}$ strength were included in the $1d_{3/2}$ shell. In the IPSM the 18 protons (22 neutrons) of ^{40}Ar fill the shells up to the $1d_{3/2}$ ($1f_{7/2}$) shell and the occupancies of the shells are not measured. For ^{40}Ar we assume the same occupancies of the orbitals as for ^{40}Ca because the structures of these nuclei are almost identical.

In our approach the occupancy of the IPSM orbitals of ^{40}Ca and ^{40}Ar are approximately 87% on average. We assume that the missing strength can be attributed to the short-range NN correlations, leading to the appearance of the high-momentum and high-energy nucleon distribution in the target. We use the general expression [53] for the high-momentum part of the spectral function P_{HM} with the parametrization of the momentum distribution for ^{40}Ca taken from Ref. [54]. In our calculations, the spectral function P_{HM} incorporates 13% of the IPSM sum-rule limit. The inclusive cross sections with the FSI effects in the presence of the short-range NN correlations were calculated using the approach proposed in Ref. [33]. To

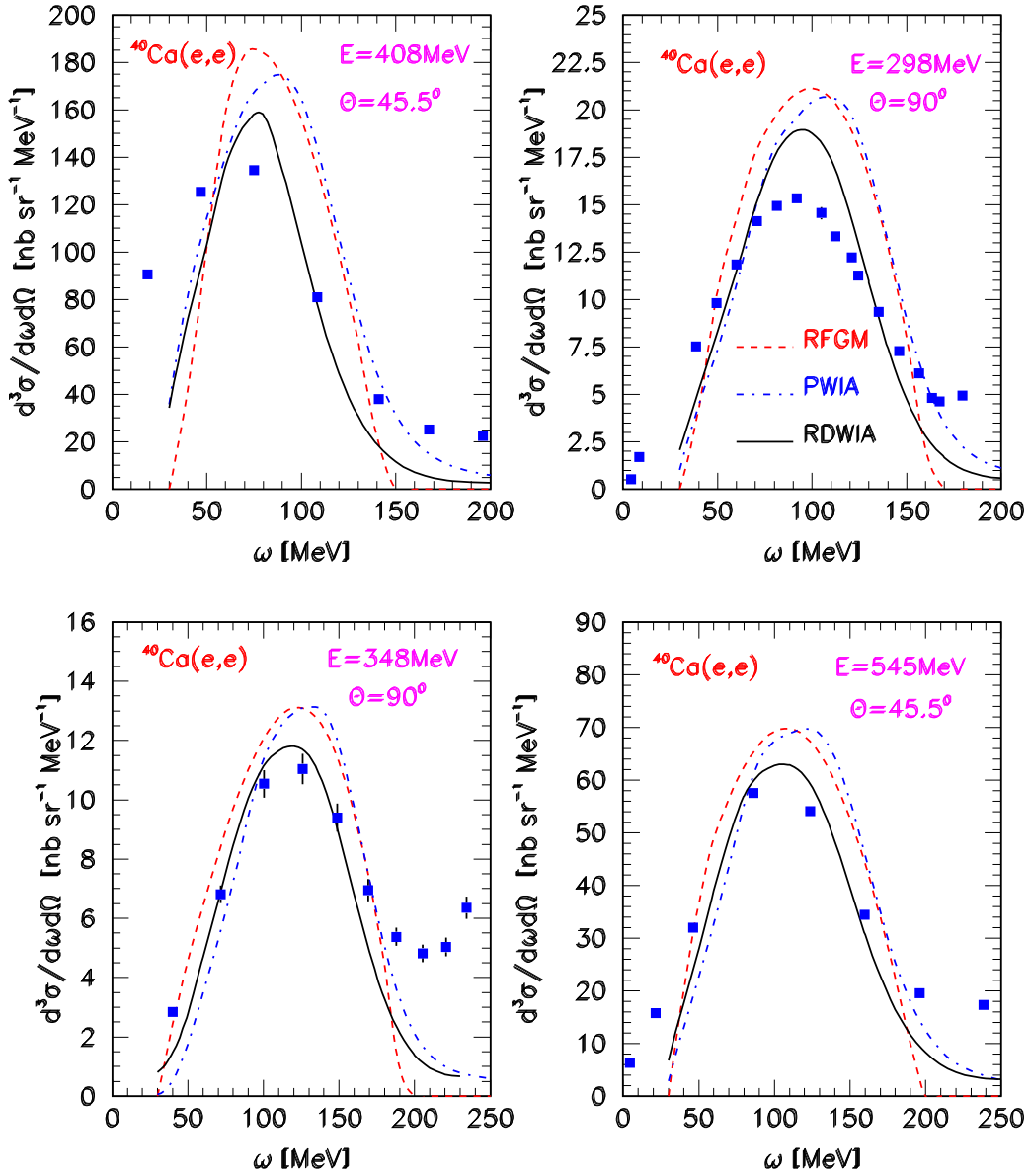


FIG. 3: (Color online) Inclusive cross section versus energy transfer ω for electron scattering on ⁴⁰Ca. The data are from Ref.[30] for the electron beam energies $E_e=408, 545$ MeV and scattering angle $\theta=45.5^\circ$; $E_e=298, 348$ MeV and $\theta=90^\circ$. As shown in the the key, cross sections were calculated with the RDWIA, PWIA, and RFGM.

test our approach, we calculated the inclusive ⁴⁰Ca(e, e') cross sections and compared them with data from SLAC [26] and Bates [30] experiments. Figures 3 and 4 show measured inclusive cross sections as functions of energy transfer as compared to the RDWIA, PWIA, and relativistic Fermi gas model (RFGM) calculations with the Fermi momentum $p_F=249$

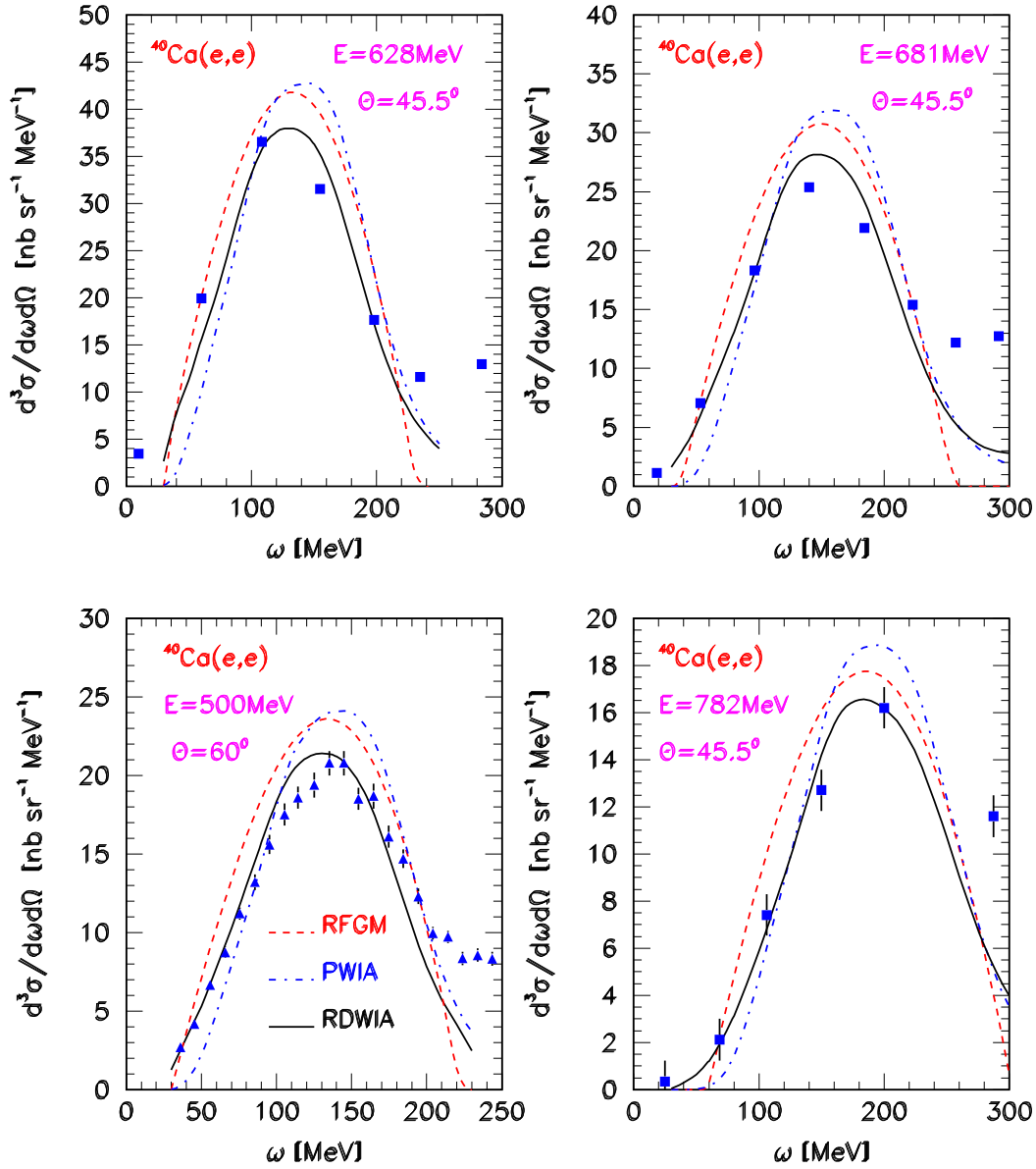


FIG. 4: (Color online) Same as Fig. 3, but the data are from Ref. [30] (squares) for $E_e=628, 681, 782$ MeV, $\theta=45.5^\circ$ and from Ref.[26] (triangles) for $E_e=500$ MeV, $\theta=60^\circ$.

MeV and nuclear binding energy $\epsilon_b=33$ MeV. These data cover the range of the three-momentum transfer (around the peak) from $|\mathbf{q}| \approx 300$ MeV/c (beam energy $E_e=408$ MeV and scattering angle $\theta = 45.5^\circ$ up to $|\mathbf{q}| \approx 560$ MeV/c ($E_e=782$ MeV, $\theta = 45.5^\circ$). We note that relative to the PWIA results, the generic effect of the FSI reduces the cross section value around the QE peak and shifts the peak toward lower values of the energy transfer. The peak in the RDWIA calculation occurs at the same energy loss as the data and the

value of the calculated cross sections (apart from $E_e=298$ MeV, $\theta = 90^\circ$) generally agree with data within 14%. On the other hand the PWIA and RFGM results systematically overestimate the data.

B. Neutrino scattering

To study nuclear effects on the Q^2 distribution, we calculated with $M_A=1.032$ GeV the inclusive cross sections $d\sigma/dQ^2$ for (anti)neutrino energies $\varepsilon_\nu=0.5, 0.7, 1.2$ and 2.5 GeV in the RDWIA and RFGM approaches. The results for neutrino and antineutrino scattering on calcium and argon are presented in Figs. 5 and 6, respectively, which show $d\sigma/dQ^2$ as functions of Q^2 scaled with the number of neutron/proton in the target (cross section per neutron/proton). Here, the results for calcium obtained in the RDWIA, are compared with cross sections calculated in the RFGM. The cross sections for ^{40}Ca and ^{40}Ar are almost identical. At the maximum the Fermi gas model results for neutrino (antineutrino) are higher than those obtained within the RDWIA. The discrepancy equals to 13% (20%) for $\varepsilon_\nu=0.5$ GeV and decreases to 7% (12%) for $\varepsilon_\nu=2.5$ GeV. The neutrino and antineutrino total cross sections for CCQE scattering off ^{40}Ca and ^{40}Ar , calculated in the RDWIA and RFGM approaches with $M_A=1.032$ GeV are shown in Fig. 7 together with data from Refs.[55–60]. Also shown are the total cross sections of the exclusive single-nucleon knock out ($\nu_\mu, \mu^- p$) and ($\bar{\nu}_\mu, \mu^+ n$) channels for (anti)neutrino scattering from on-shell nucleons. These reactions are source of the CCQE two-particle events in the final states. The cross sections are scaled with the number of neutron/proton in the target.

The ratio between the neutrino cross sections calculated in the RFGM and RDWIA decreases with neutrino energy from about 1.26 for $\varepsilon_\nu=0.3$ GeV to ≈ 1.16 for $\varepsilon_\nu=1$ GeV and down to ≈ 1.09 for $\varepsilon_\nu=2.4$ GeV. For antineutrino cross sections this ratio is about 2.17 for $\varepsilon_\nu=0.3$ GeV, 1.3 for $\varepsilon_\nu=1$ GeV and 1.16 for $\varepsilon_\nu=2.4$ GeV. The calculated results show significant nuclear-model dependence for energy about 2 GeV or less.

From the experimental data shown in Fig.7 one can conclude that the CCQE total cross sections measured in different experiments can vary by 20-40%. The data have large systematic uncertainties due to the poor knowledge of the background contamination in selected events and/or the incoming neutrino flux. Obtaining a reliable estimate of the neutrino flux is notoriously difficult and remains a challenge.

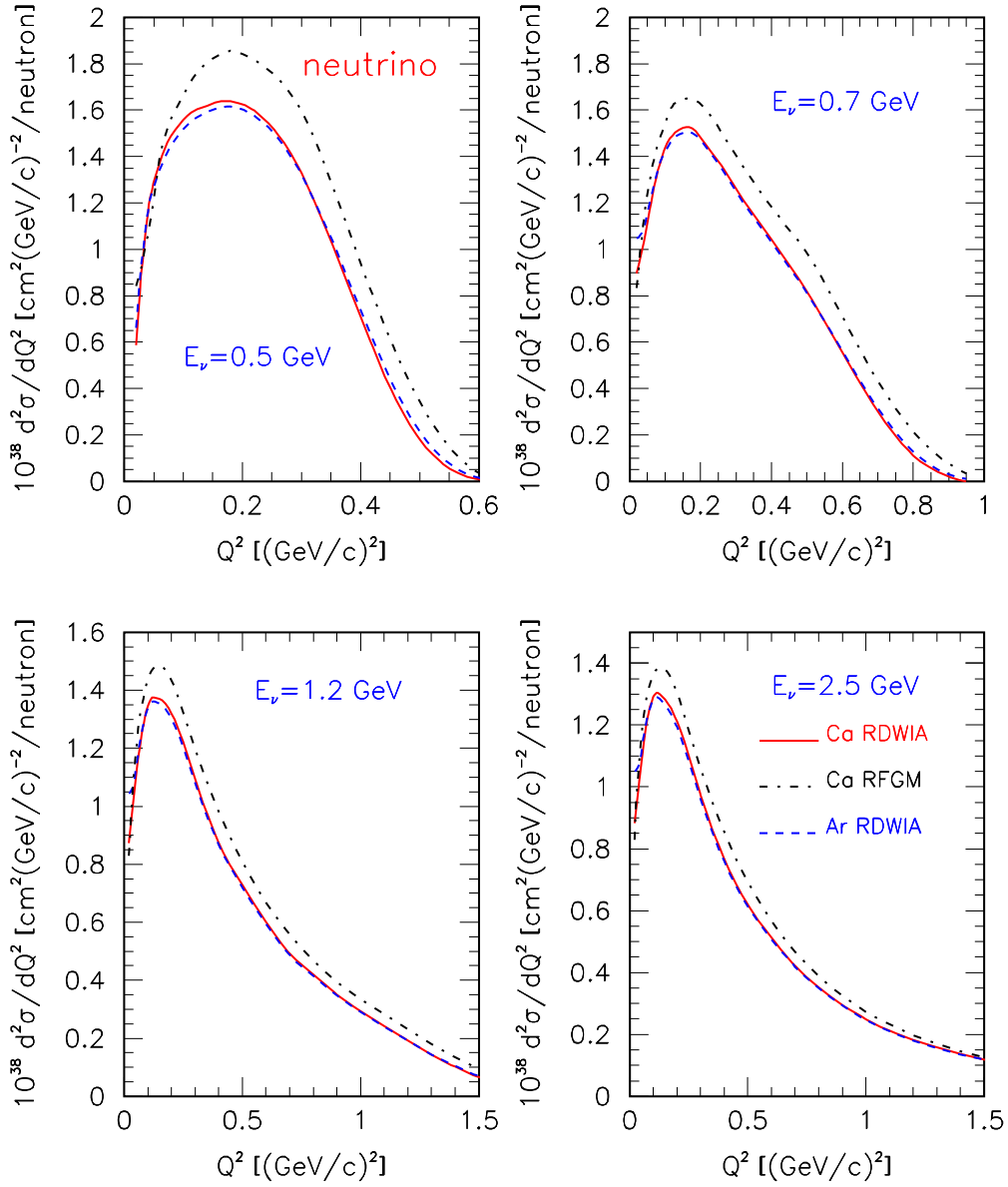


FIG. 5: (Color online) Inclusive cross section per neutron vs. the four-momentum transfer Q^2 for neutrino scattering on ^{40}Ca and ^{40}Ar and for the four values of incoming neutrino energy: $\varepsilon_\nu = 0.5, 0.7, 1.2,$ and 2.5 GeV . As shown in the key, the cross sections were calculated with the RDWIA and RFGM (for calcium) approaches.

Selection techniques that rely on the identification of a single final state proton (two track CCQE events) can improve significantly the purity of the QE sample. Moreover, a simultaneous measurement of both two track and single muon track events [6] allow to constrain the systematics associated with the FSI and the neutrino flux. The ratio of the exclusive

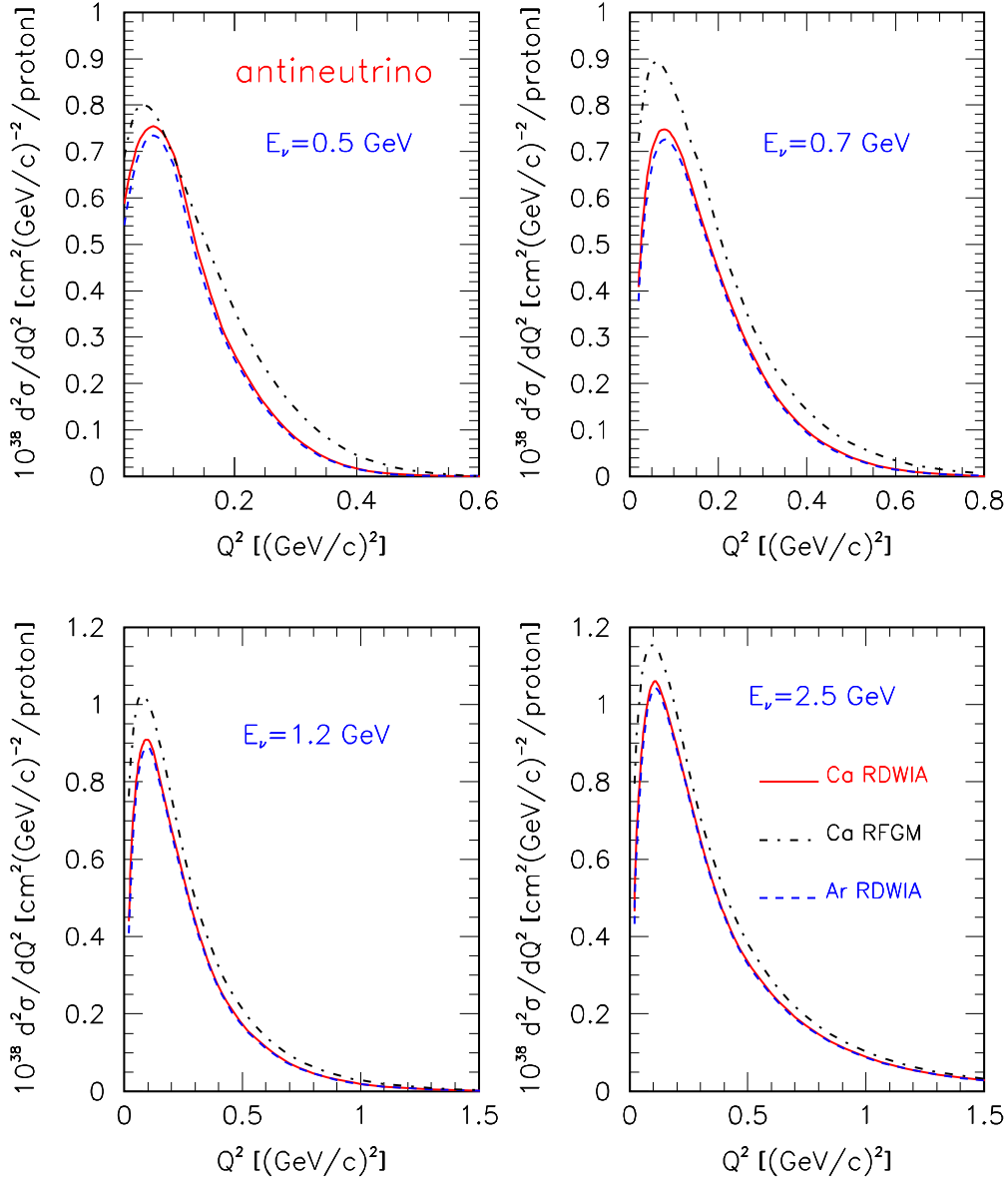


FIG. 6: (Color online) Same as Fig. 5, but cross section per proton for antineutrino scattering.

$(\nu_{\mu}, \mu^{-}p)$ reaction total cross section to the CCQE total cross section is an attractive quantity because it is supposed to be rather insensitive to the neutrino flux uncertainty and can be especially susceptible to the FSI effects.

We calculated the $R^{ex} = \sigma_{tot}^{ex}/\sigma_{tot}$ ratio, where σ_{tot}^{ex} is the total cross section of the $(\nu_{\mu}, \mu N)$ reaction for the (anti)neutrino scattering on shell-nucleons on the carbon [35], oxygen [33] and argon. The results calculated in the RDWIA are shown in Fig. 8 as functions of (anti)neutrino energy. This figure clearly shows that the ratio reduces with the

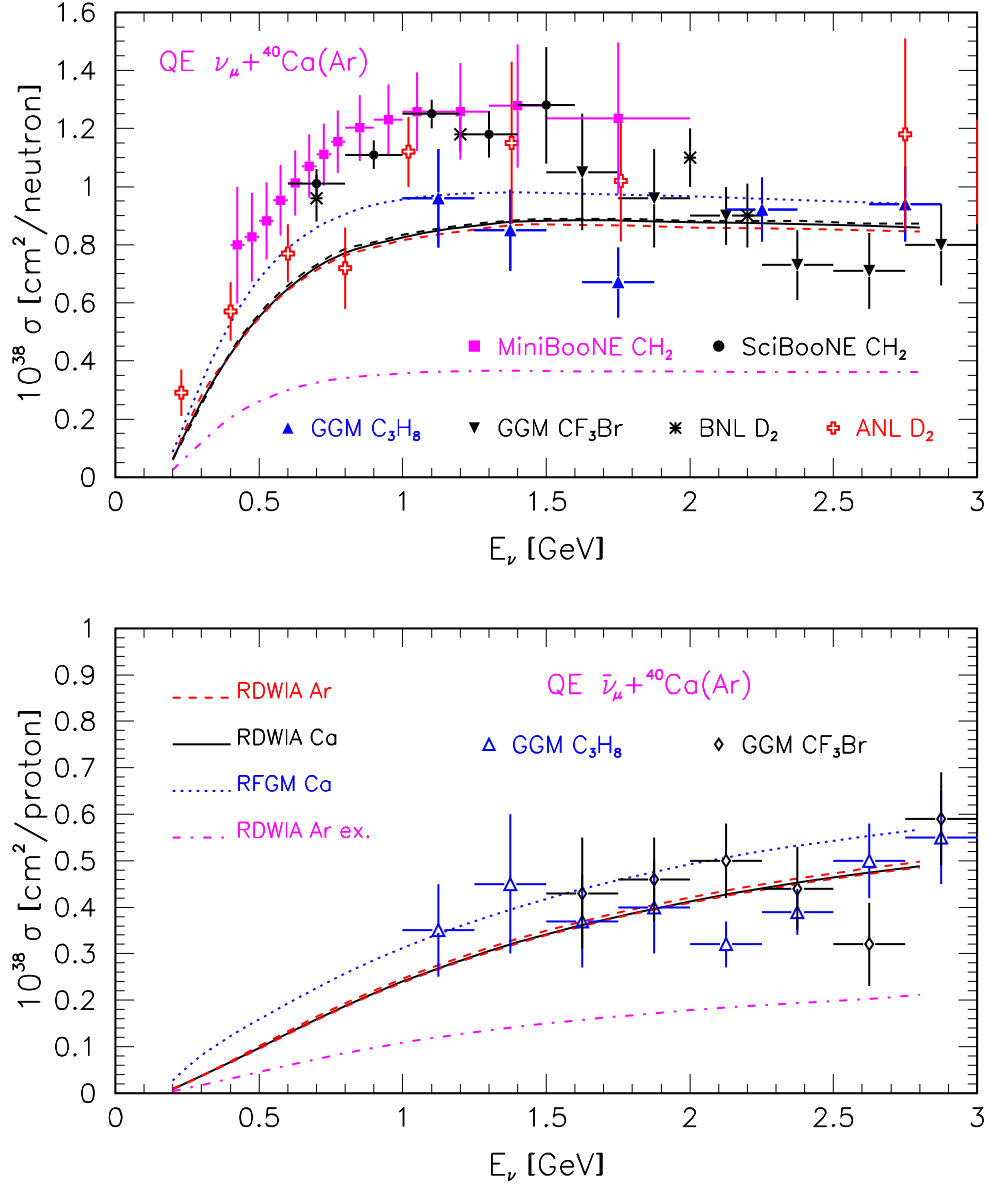


FIG. 7: (Color online) Total cross section for CCQE scattering of muon neutrino (upper panel) and antineutrino (lower panel) on ${}^{40}\text{Ca}$ and ${}^{40}\text{Ar}$ as a function of incoming (anti)neutrino energy. The solid and dashed lines are the RDWIA results for calcium and argon, respectively, while the dotted line is the RFGM calculation. The dashed-dotted line is the RDWIA result for exclusive $(\nu, \mu N)$ reactions. Data points for different targets are from Refs.[55–60]

mass number of the target. The function $R^{ex}(\varepsilon_\nu)$ has a maximum in the range $\varepsilon_\nu=0.3-0.4$ GeV and decreases slowly with neutrino energy. For carbon (oxygen) (argon) the ratio is 0.59 (0.55) (0.48) at the maximum and ≈ 0.54 (0.46) (0.43) at $\varepsilon_\nu=2.8$ GeV. So, due to the FSI the contribution of the exclusive channels reduces slowly with the neutrino energy and mass-number of the target.

Most long base-line neutrino oscillation experiments try to reduce systematic errors in the extraction of the oscillation parameters by using near and far detectors. Because these detectors are not necessarily of the same target material we estimated the difference between the total cross sections per (proton)neutron for the (anti)neutrino CCQE scattering off ^{12}C , ^{16}O , and ^{40}Ar . The ratio $R(\varepsilon_\nu) = (\sigma_{tot}^{Ar})_{nucl}/(\sigma_{tot}^C)_{nucl}$ (Ar/C ratio) was calculated, where the cross sections $(\sigma_{tot}^i)_{nucl}$ are scaled with the number of neutron/proton in the target. The results obtained in the RFGM and RDWIA are shown in Fig.9. The ratio $R(\varepsilon_\nu = (\sigma_{tot}^O)_{nucl}/(\sigma_{tot}^C)_{nucl})$ (O/C ratio) calculated in Ref. [35] is also shown for comparison.

The Fermi gas model predicts almost identical values of σ_{tot}^O and σ_{tot}^C . For neutrino (antineutrino) scattering the ratio Ar/C increases from 0.89(0.84) at $\varepsilon_\nu=0.3$ GeV up to 0.99(0.98) at $\varepsilon_\nu=2.8$ GeV. In the RDWIA approach the ratios O/C and Ar/C are lower than those calculated in the RFGM. For the neutrino(antineutrino) scattering O/C is 0.88(0.85) at $\varepsilon_\nu=0.5$ GeV and increases slowly with energy up to 0.93(0.92) at $\varepsilon_\nu=2.8$ GeV. On the other hand Ar/C ratio of 0.95(0.75) at $\varepsilon_\nu=0.5$ GeV decreases with energy up to 0.88 for the neutrino interaction and increases up to 0.88 for the antineutrino scattering at $\varepsilon_\nu=2.8$ GeV.

In the SLAC experiments the inclusive cross sections $d\sigma/d\varepsilon d\Omega$ for electron scattering on ^{12}C and ^{16}O [61] as well as on ^{12}C and ^{16}O [26] were measured in the same kinematical conditions. Using these data we calculated the $(O/C)_{el} = (d\sigma^O/d\varepsilon d\Omega)_{nucl}/(d\sigma^C/d\varepsilon d\Omega)_{nucl}$ and $(Ca/C)_{el} = (d\sigma^{Ca}/d\varepsilon d\Omega)_{nucl}/(d\sigma^C/d\varepsilon d\Omega)_{nucl}$ ratios, where the differential cross sections $(d\sigma^i/d\varepsilon d\Omega)_{nucl}$ are scaled with the number of nucleons in the targets. Figures 10 and 11 show the measured ratios as functions of energy transfer as compared to the RDWIA calculations in the QE peak region.

There is an agreement between the RDWIA results and the $(O/C)_{el}$ data within the error of the experiments, whereas the uncertainties of the measured $(O/C)_{el}$ ratios of 5-10% are the same order as the predicted effects. On the other hand the calculated $(Ca/C)_{el}$ ratio agree well with data where the observed effect of 15% in the QE peak region is higher than

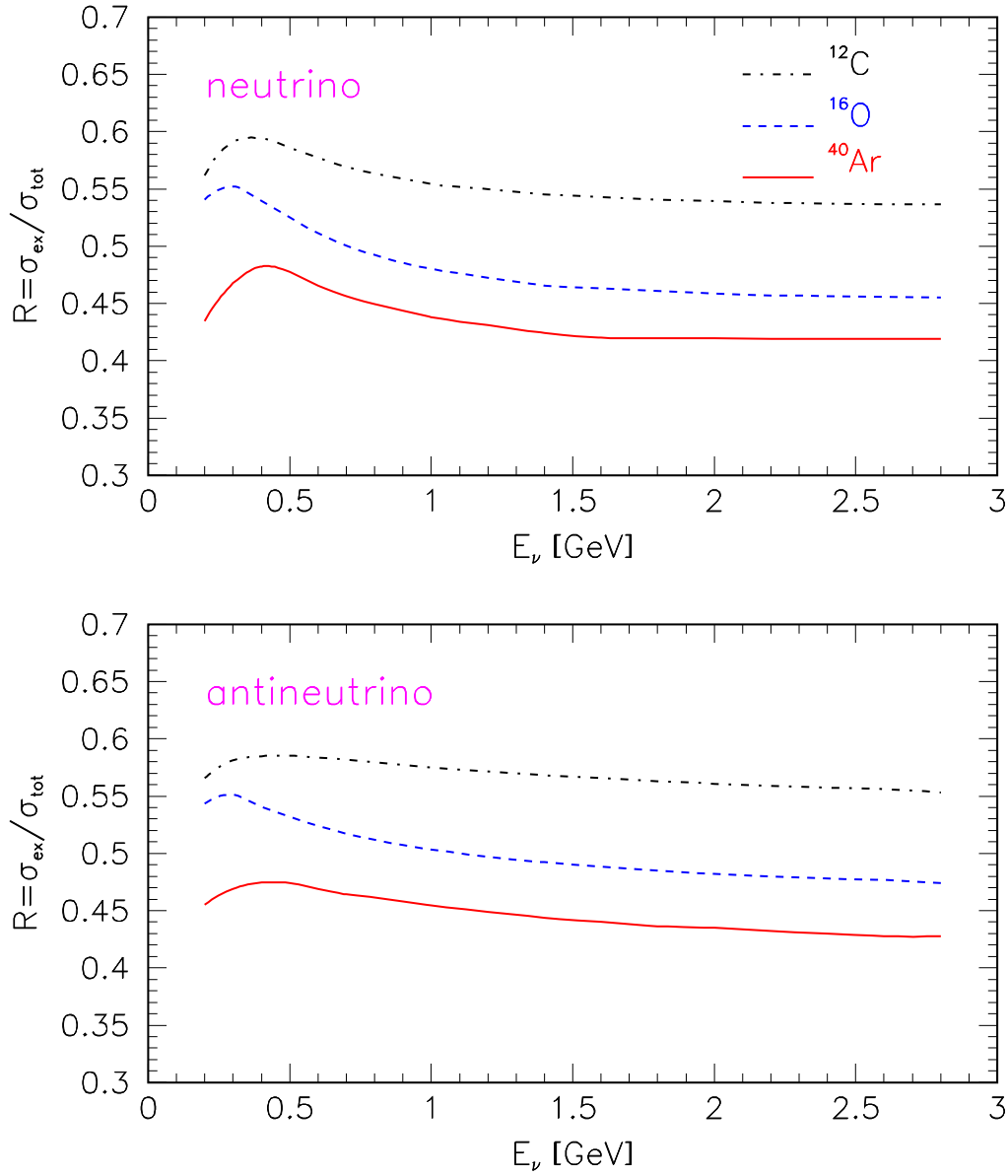


FIG. 8: (Color online) Ratio R^{ex} of the $(\nu_\mu, \mu N)$ reaction total cross section to the CCQE total cross section for muon neutrino (upper panel) and antineutrino (lower panel) scattering on ^{12}C (dashed-dotted line), ^{16}O (dashed line), and ^{40}Ar (solid line) vs incoming (anti)neutrino energy. The ratio was calculated in the RDWIA approach.

experimental errors. Thus the RDWIA model predicts that due to nuclear effects the CCQE differential and total cross sections per neutron/proton reduces with the mass number of the targets.

To investigate why the (anti)neutrino CCQE total cross sections per neutron/proton

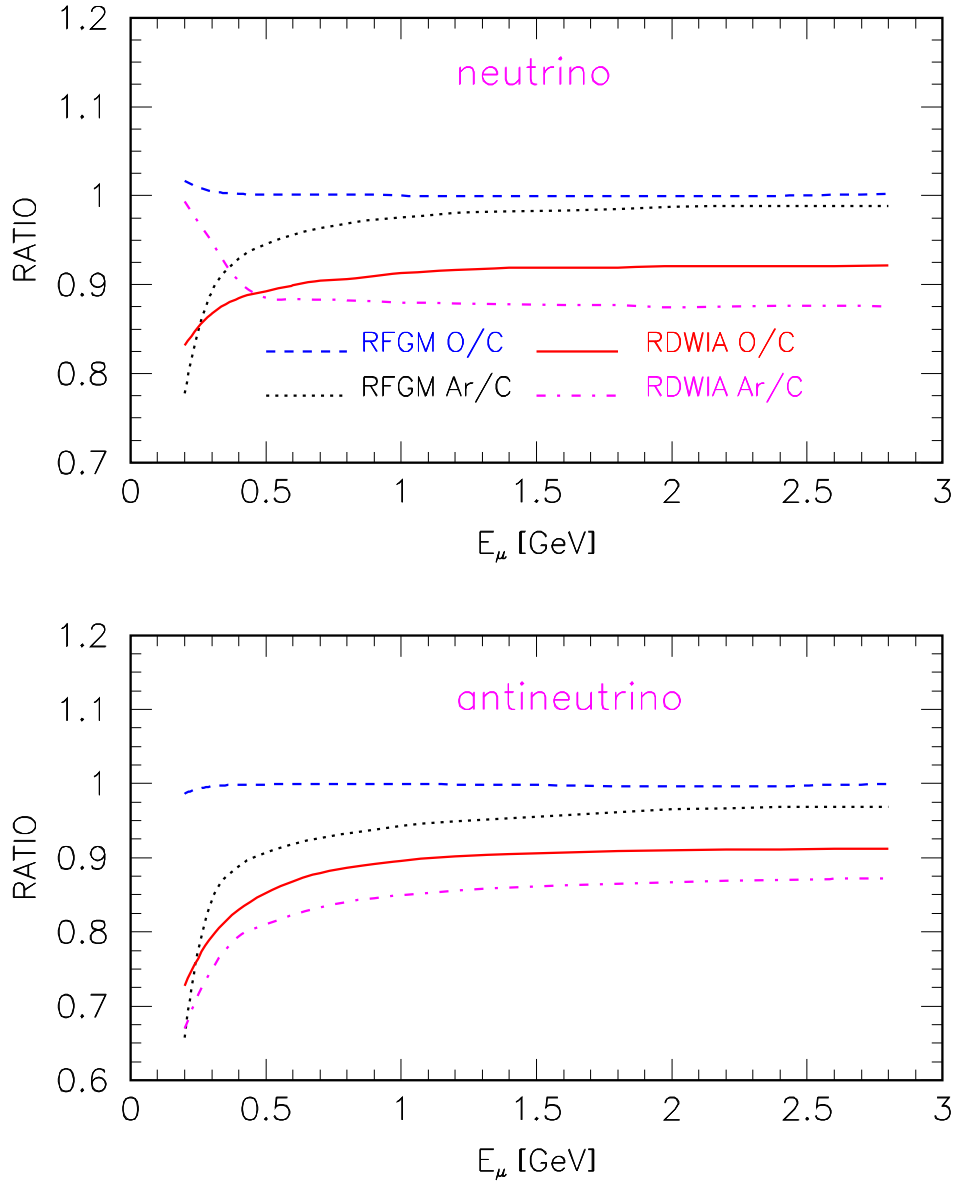


FIG. 9: (Color online) Ratio of the total cross sections per neutron/proton $R = O/C$ (solid and dashed lines) [35] and $R = Ar/C$ (dashed-dotted and dotted lines) for CCQE scattering of muon neutrino (upper panel) and antineutrino (lower panel) as a function of incoming (anti)neutrino energy. As shown in the key, the cross sections were calculated with the RDWIA and RFGM approaches.

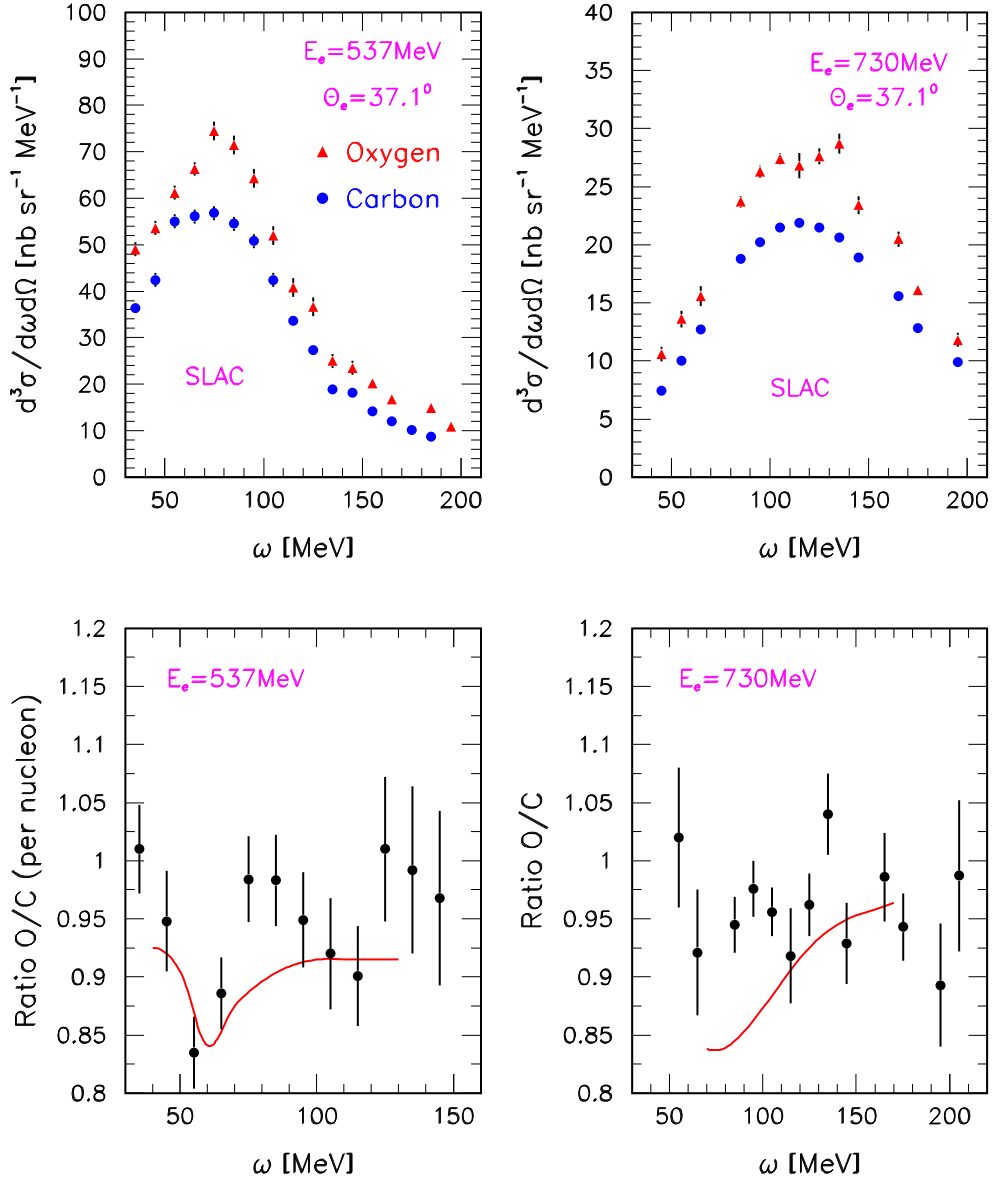


FIG. 10: (Color online) Inclusive cross sections (upper panel) per nucleon and ratio O/C (lower panel) vs energy transfer ω for electron scattering on ^{12}C and ^{16}O . Data for carbon (filled circles) and oxygen (filled triangles) are from Ref. [61] for electron beam energies $\varepsilon_e = 537, 730$ MeV and scattering angle $\theta_e = 37.1^\circ$. The solid line is the RDWIA calculation.

for ^{12}C , ^{16}O , and ^{40}Ar are dissimilar we estimated the nuclear structure, short-range NN correlation, and FSI effects.

The nuclear structure effects are different in ^{16}O (^{40}Ar) and ^{12}C cross sections due to different nucleon binding energies and momentum distributions for all bound nucleon states

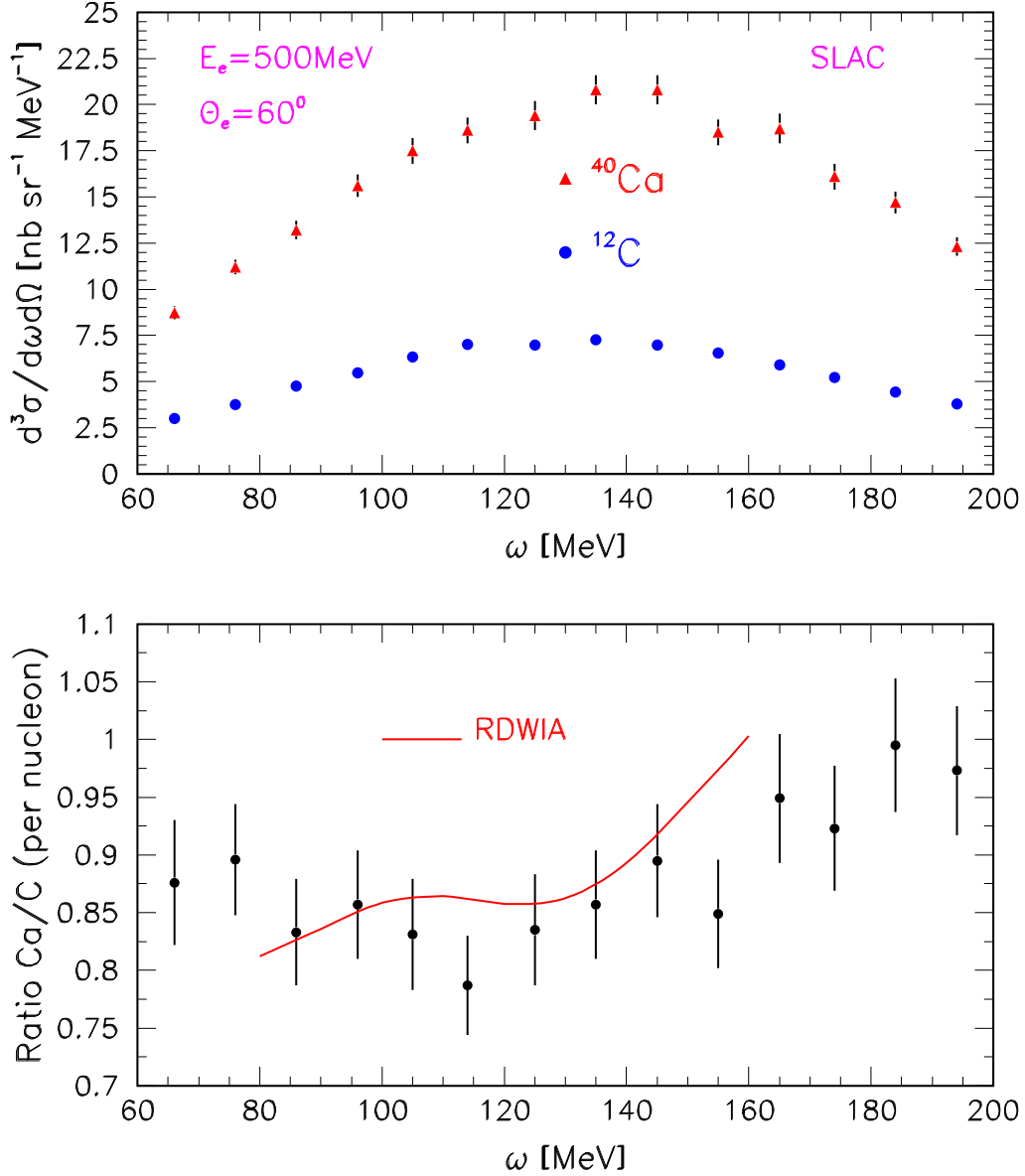


FIG. 11: (Color online) Inclusive cross sections (upper panel) per nucleon and ratio Ca/C (lower panel) vs. energy transfer ω for electron scattering on ^{12}C and ^{40}Ca . Data for carbon (filled circles) and calcium (filled triangles) are from Ref. [26] for electron beam energies $\varepsilon_e=500$ MeV and scattering angle $\theta_e=60^\circ$. The solid line is the RDWIA calculation.

in these nuclei. To estimate these effects we calculated the ratios $R_{str}(\varepsilon_\nu) = O/C(Ar/C)$ in the PWIA approach without the NN pair contributions, assuming that the occupancy of all nuclear shells $S_\alpha=1$ in carbon, oxygen and argon. The nuclear structure effect was estimated as $\Delta_{str}=1 - R_{str}$. Then we calculated in the same approach the $R_{NN}(\varepsilon_\nu)$ ratios in

the presence of the NN correlations in the ground states of nuclei. Note, in our calculations the averaged occupancies of the IPSM orbitals of ^{12}C , ^{16}O , and ^{40}Ar are: $S_C=0.89$, $S_O=0.75$, and $S_{Ar}=0.87$. The NN correlation effect, i.e. the difference between the cross sections as a consequence of different NN pair contributions was calculated as $\Delta_{NN}=R_{str} - R_{NN}$. The FSI effects are different between the cross sections due to interaction of the outgoing nucleons with the different residual nuclei. For example, $p + ^{11}\text{C}$ for the neutrino or $n + ^{11}\text{B}$ for the antineutrino scattering off the ^{12}C and $p + ^{15}\text{O}$ for the neutrino and $n + ^{15}\text{N}$ for the antineutrino scattering off ^{16}O . These effects were estimated as the difference $\Delta_{FSI}=R_{NN} - R$, where the ratio R is calculated in the RDWIA approach is shown in Fig. 9 and 10. The total nuclear effect is sum $\Delta_{tot}=\Delta_{str} + \Delta_{NN} + \Delta_{FSI} = 1 - R$.

The result of the cross section comparison for the (anti)neutrino scattering on carbon and oxygen as well as on carbon and argon is displayed in Figs. 12 and 13, correspondingly. In these figures the differences Δ_{str} , Δ_{NN} , Δ_{FSI} and Δ_{tot} are shown as functions of neutrino energy. Comparison of the cross sections for ^{12}C and ^{16}O shows that the nuclear structure effects for the neutrino and antineutrino interactions are small and similar. The function Δ_{str} increases slowly with energy up to $\approx 2\%$ at $\varepsilon_\nu=2.8$ GeV. The NN correlation effects decrease with increased (anti)neutrino energy. For the neutrino(antineutrino) scattering the function $\Delta_{NN}(\varepsilon_\nu)$ reduces from $\approx 8\%(7\%)$ at $\varepsilon_\nu=0.5$ GeV up to $\approx 4\%(4\%)$ at $\varepsilon_\nu=2.8$ GeV. The FSI effects are higher for the antineutrino scattering than those for the neutrino interaction. For the neutrino (antineutrino) scattering the function $\Delta_{FSI}(\varepsilon_\nu)$ decreases from $\approx 3\%(9\%)$ at $\varepsilon_\nu=0.5$ GeV down to $\approx 2\%(3.5\%)$ at $\varepsilon_\nu=2.8$ GeV and the total nuclear effect $\Delta_{tot}(\varepsilon_\nu)=0.11(0.17)$ at $\varepsilon_\nu=0.5$ GeV and reduces down to $0.08(0.09)$ at $\varepsilon_\nu=2.8$ GeV.

To conclude, the main sources of the distinction between the carbon and oxygen cross sections are different NN pair contributions in the ^{12}C (11%) and ^{16}O (25%) ground states. For the antineutrino cross sections the FSI effects are the same order as NN correlation effects at $\varepsilon_\nu \geq 1$ GeV. The precise measurement and accurate calculation of the NN correlation contributions are important for a reliable estimation of the difference between the ^{12}C and ^{16}O cross sections.

Comparison of the cross sections for ^{12}C and ^{40}Ar shows that the nuclear structure effects at $\varepsilon_\nu \geq 0.5$ GeV are identical for neutrino and antineutrino interactions. The function $\Delta_{str}=0.06$ at $\varepsilon_\nu=0.5$ GeV and increases slowly with energy up to ≈ 0.07 at $\varepsilon_\nu=2.8$ GeV. The NN correlation effects of 1-2% are small. The FSI effects are higher for the antineutrino

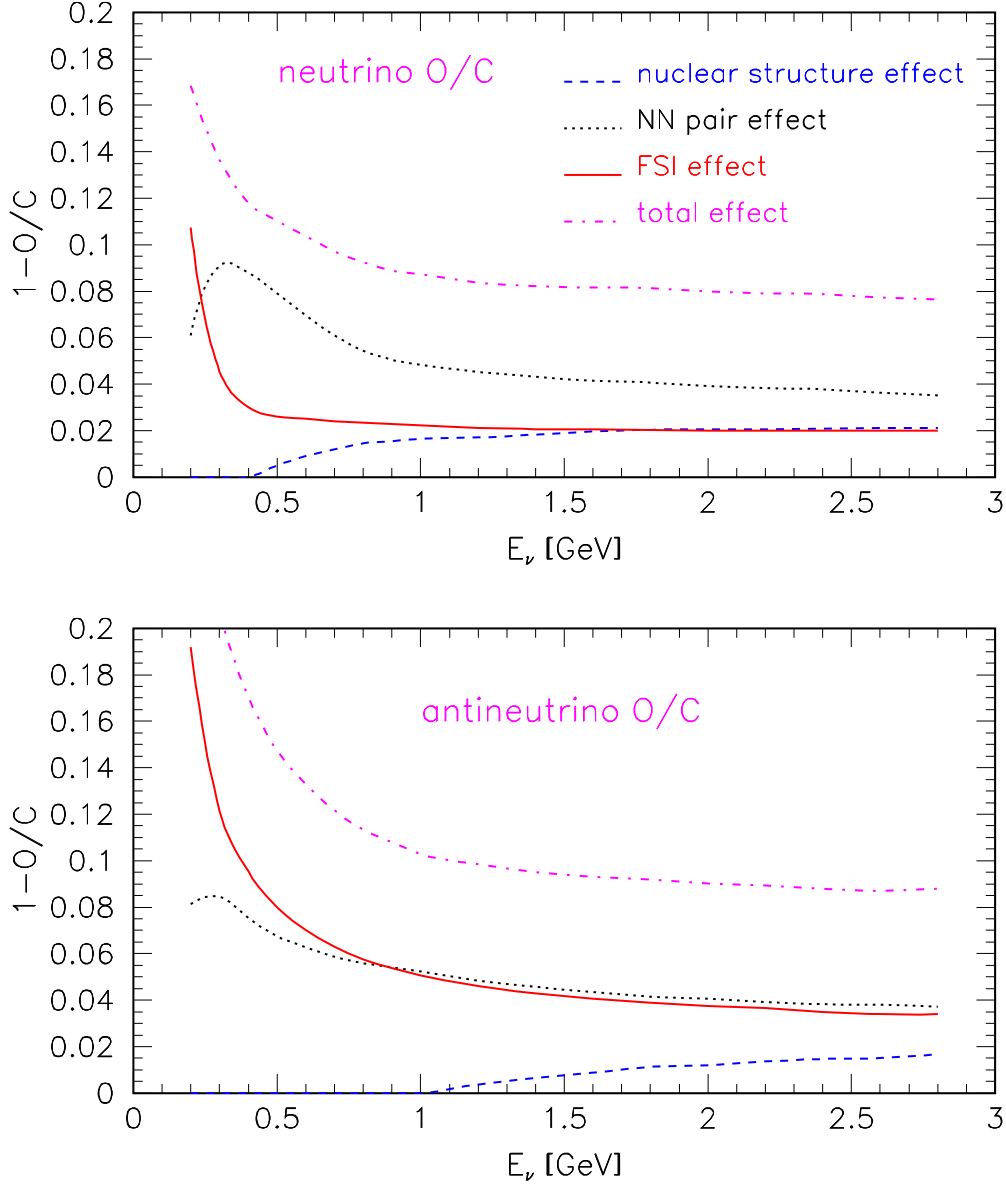


FIG. 12: (Color online) Nuclear structure (dashed line), NN correlation (dotted line), FSI (solid line), and total nuclear effects (dashed-dotted) (see text) for CCQE scattering of muon neutrino (upper panel) and antineutrino (lower panel) on ^{12}C and ^{16}O vs incoming (anti)neutrino energy.

scattering. For the neutrino (antineutrino) interaction Δ_{FSI} is about 0.045(0.13) for $\varepsilon_\nu=0.5$ GeV and reduces with energy down to 0.035(0.06) for $\varepsilon_\nu=2.8$ GeV and the total nuclear effect $\Delta_{tot}=0.12$ (0.18) at $\varepsilon_\nu=0.5$ GeV and ≈ 0.13 (0.13) at $\varepsilon_\nu=2.8$ GeV. Thus the nuclear structure and FSI effects give the dominant contribution to the difference between the ^{12}C and ^{40}Ar total cross sections per neutron/proton.

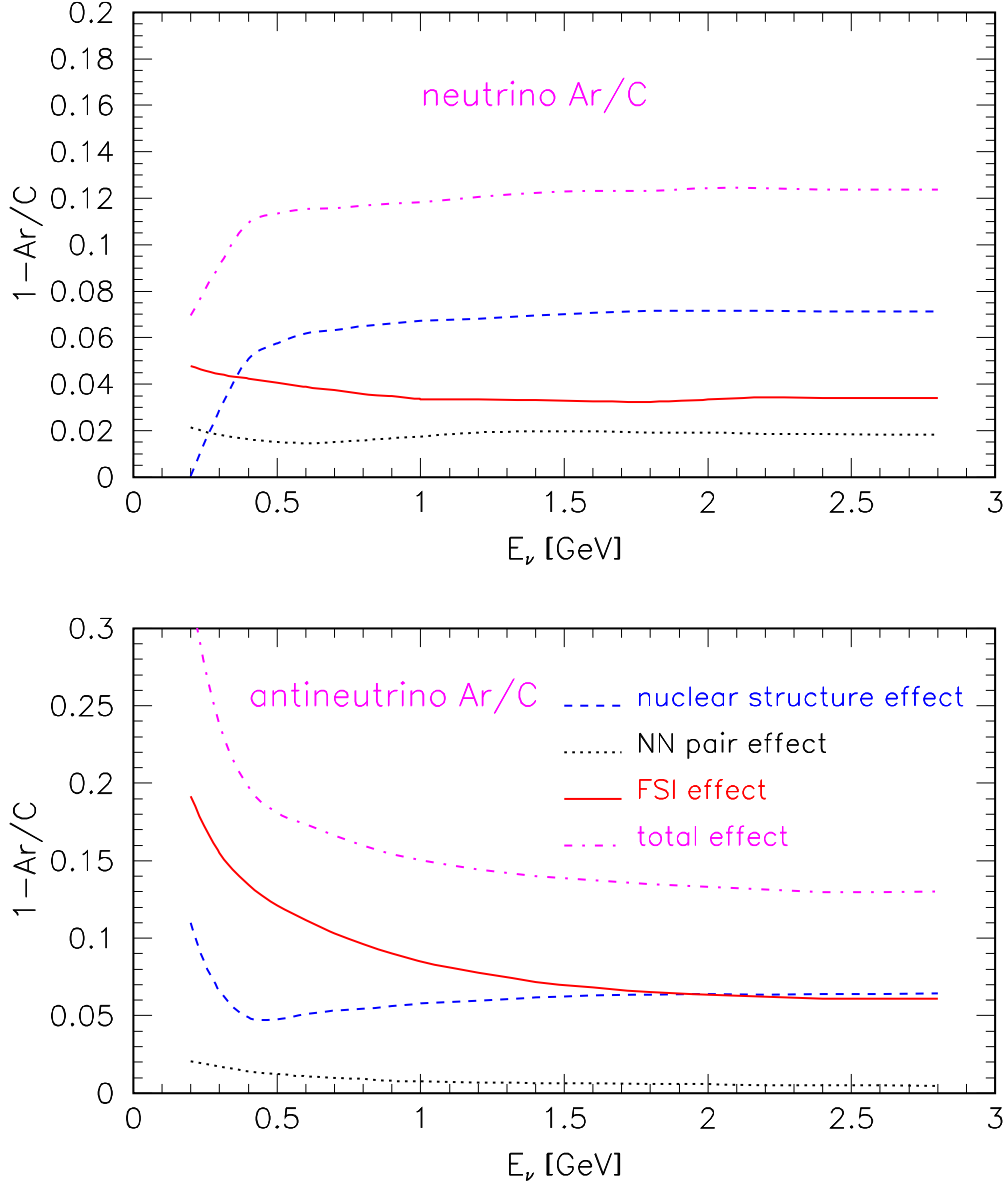


FIG. 13: (Color online) Same as Fig.12 but for (anti)neutrino scattering on ^{12}C and ^{40}Ar .

IV. CONCLUSIONS

In this work, we study electron and CCQE (anti)neutrino scattering on calcium and argon targets in different approaches (PWIA, RDWIA, RFGM). The RDWIA model were widely and successfully applied to the analysis of the available electron scattering data over a wide range of nuclei.

First, the reduced cross sections for electron and (anti)neutrino scattering off ^{40}Ca cal-

culated in the RDWIA were tested against $^{40}\text{Ca}(e, e'p)$ data. We found that the result for (anti)neutrino scattering are similar to those for electron scattering (apart from the small differences due to the Coulomb correction) and the latter are in good agreement with the electron data. Also it was shown that the reduced cross sections for the removal of the proton from the shells of ^{40}Ca and ^{40}Ar are very similar.

The inclusive cross sections, calculated in the RDWIA model, which has been modified with phenomenological spectroscopic factors and nucleon high-momentum components in the target were tested against $^{40}\text{Ca}(e, e')$ data. The results generally agree within about 14%. On the other hand, in the QE peak region the RFGM overestimates the value of the inclusive cross sections at low momentum transfer and the discrepancy with data reduces as this momentum increases. Also, it was shown that the measured and calculated in the RDWIA inclusive cross sections per nucleon for electron scattering off ^{12}C , ^{16}O , and ^{40}Ca decreases with the mass-number of the target in the QE peak region.

The CCQE total cross sections for (anti)neutrino scattering on calcium and argon predicted by the RFGM are higher than those obtained in the RDWIA and the difference decreases with (anti)neutrino energy. The relative contribution of the $(\nu_\mu, \mu N)$ channels to the CCQE total cross section is lower for heavier nuclei due to the FSI and NN pair effects. For (anti)neutrino scattering on carbon, oxygen, and argon we compared the total cross sections (scaled with the number of neutrons/protons in the target) and found that the cross sections calculated within the RDWIA for ^{16}O and ^{40}Ar are lower than those calculated for ^{12}C . In the RFGM the cross sections for carbon are practically equal to those for oxygen and they are higher by about 2-5% than those for argon at $\varepsilon \geq 0.5$ GeV.

We also studied different sources of the distinction between the ^{12}C , ^{16}O , and ^{40}Ar cross sections per neutron/proton. We have found that the difference between the ^{12}C and ^{16}O cross sections is mainly due to different NN correlation contributions in the ground states of the nuclei and FSI effects. The main sources of the difference between the ^{12}C and ^{40}Ar cross sections are the nuclear structure and FSI effects.

Thus the RDWIA approach predicts that the CCQE differential and total cross sections per neutron/proton reduces slowly with the mass-number of the target due to the nuclear effects. Although the model and theoretical ingredients adopted in the calculations contain approximations, our results can serve as a useful reference for long base-line neutrino oscillation experiments

Acknowledgments

We thank L. Lapikás for providing the NIKHEF data tables. We especially thank J. Morfin, B. Ziemer and D. Perevalov for fruitful discussions and a critical reading of the manuscript. The support of the Russian Academy of Science is gratefully acknowledged.

-
- [1] R. Gran *et al.*, Phys. Rev. Lett. **D74**, 052002 (2006).
 - [2] AK.Hiraide *et al.*, (SciBooNE Collaboration), Phys.Rev. **D78**, 112004 (2008).
 - [3] K. S. McFarland, AIP Conf. Proc **1405**, 362 (2011).
 - [4] A. Ferrero, AIP Conf. Proc **1189**, 77 (2009).
 - [5] B. Rebel, AIP Conf. Proc **1382**, 88 (2011).
 - [6] V. Lyubushkin *et al.*, Eur. Phys. J. **C63**, 355 (2009).
 - [7] S. Amerio *et al.*, Nucl. Instrum. Meth. **A527**, 329 (2004).
 - [8] M. Soderberg, AIP Conf. Proc **1189**, 83 (2009).
 - [9] T. Akiri *et al.*, arXiv:1110.6249 [hep-ex]
 - [10] M. Anghinolfi *et al.*, J. Phys. G.: Nucl. Part. Phys. **21**, L9 (1995).
 - [11] K. Nakamura, S. Hiramatsu, T. Kamae, N. Izutsu, and Y. Watase, Phys. Rev. Lett.**33**, 853 (1974).
 - [12] K. Nakamura, S. Hiramatsu, T. Kamae, N. Izutsu, and Y. Watase, Nucl. Phys. **A271**, 221 (1976).
 - [13] J. Mougey *et al.*, Nucl. Phys. **A262**, 461 (1976).
 - [14] G. J. Kramer, PhD thesis, University of Amsterdam, 1990 (unpublished).
 - [15] G. J. Kramer *et al.*, Phys. Lett. **B227**, 199 (1989).
 - [16] G. J. Kramer, H. P. Blok, and L. Lapikas, Nucl. Phys. **A679**, 267 (2001).
 - [17] C. Giusti, and F. D. Pacati, Nucl. Phys. **A473**, 717 (1987).
 - [18] C. Giusti, and F. D. Pacati, Nucl. Phys. **A485**, 461 (1988).
 - [19] J. J. Kelly, Adv. Nucl. Phys. **23**, 75 (1996).
 - [20] L. Lapikas, Nucl. Phys. **A553**, 2970 (1993).
 - [21] J. P. McDermott, Phys. Rev. Lett. **65**, 1991 (1990).
 - [22] Y. Jin, D. S. Onley, and L. E. Wright, Phys. Rev. **C45**, 1311 (1992).

- [23] J. M. Udias, P. Sarriguren, E. Moya de Guerra, E. Garrido, and J. A. Caballero, Phys. Rev. **C48**, 2731 (1993).
- [24] J. M. Udias, P. Sarriguren, E. Moya de Guerra, E. Garrido, and J. A. Caballero, Phys. Rev. **C51**, 3246 (1995).
- [25] C. Giusti, A. Meucci, F. D. Pacati, G. Co', and V. De Donno, Phys. Rev. **C84**, 024615 (2011).
- [26] R. R. Whitney, I. Sick, J. R. Ficenc, R. D. Kephart, and W. P. Trower, Phys. Rev. **C9**, 2230, (1974).
- [27] Z. Meziani *et al.*, Phys. Rev. Lett. **54**, 1233 (1985).
- [28] M. Dedy, C. F. Williamson, P. D. Zimmerman, R. Altemus, R. R. Whitney, Phys. Rev. **C33**, 1897 (1986).
- [29] T. C. Yates *et al.*, Phys. Lett. **B312**, 382 (1993).
- [30] C. Williamson *et al.*, Phys. Rev. **C56**, 3152 (1997).
- [31] A. V. Butkevich and S. P. Mikheyev, Phys. Rev. **C72**, 025501 (2005).
- [32] A. M. Ankowski and J. T. Sobczyk, Phys. Rev. **C77**, 044331 (2008).
- [33] A. V. Butkevich and S. A. Kulagin, Phys. Rev. **C76**, 045502, (2007).
- [34] A. V. Butkevich, Phys. Rev. **C78**, 015501, (2008).
- [35] A. V. Butkevich, Phys. Rev. **C80**, 014610, (2009).
- [36] A. V. Butkevich, Phys. Rev. **C82**, 055501, (2010).
- [37] A. V. Butkevich and D. Perevalov, Phys. Rev. **C84**, 015501, (2011).
- [38] S. Boffi, C. Giusti, F. Pacatti, and M. Radici, *Electromagnetic Response of Atomic Nuclei (Clarendon, Oxford, 1996)*
- [39] P. Mergell, U.-G. Meissner, and D. Drechsel, Nucl. Phys. **A596**, 367, 1996.
- [40] T. de Forest, Nucl. Phys. **A392**, 232, (1983).
- [41] C. J. Horowitz and Brian D. Serot, Phys.Lett. **B86**, 146 (1979).
- [42] C. J. Horowitz and Brian D. Serot, Nucl. Phys. **A368**, 503 (1979).
- [43] C. J. Horowitz D. P. Murdock, and Brian D. Serot, in *Computational Nuclear Physics 1: Nuclear Structure* edited by K. Langanke, J. A. Maruhn, Steven E. Koonin (Springer-Verlag,Berlin, 1991), p.129.
- [44] J. J Kelly, <http://www.physics.umd.edu/enp/jjkelly/LEA>
- [45] E .D. Cooper, S. Hama, B. C. Clark, and R. L. Mercer, Phys. Rev. **C47**, 297 (1993).
- [46] J. J. Kelly, Phys. Rev. **C71**, 064610 (2005).

- [47] K. G. Fissum *et al.*, Phys. Rev. **C70**, 034606 (2004).
- [48] A. Meucci, F. Capuzzi, C. Giusti, and F. D. Pacati, Phys. Rev. **C67**, 054601 (2003).
- [49] A. Meucci, C. Giusti, and F. D. Pacati, Nucl. Phys. **A744**, 307 (2004).
- [50] <http://www.physics.umd.edu/enp/jjkelly/LEA>
- [51] W. Tornow, Z. P. Chen, J. P. Delaroche, Phys. Rev. **C42**, 693 (1990).
- [52] C. Mahaux and R. Sartor, Nucl. Phys. **A484**, 205 (1988).
- [53] S. A. Kulagin and R. Petti, Nucl. Phys. **A765**, 126 (2006).
- [54] C. Ciofi degli Atti and S. Simula, Phys. Rev. **C53** , 1689, 1996.
- [55] W. A. Mann *et al.*, Phys. Rev. Lett. **31**, 844, (1973).
- [56] N. J. Baker *et al.*, Phys. Rev. **D23**, 2499, (1981).
- [57] M. Pohl *et al.*, Lett. Nuovo Cim. **26**, 332, 1979.
- [58] J. Brunner *et al.*, Z. Phys. **C45**, 551, 1990.
- [59] A. A. Aguilar-Arevalo *et al.*, Phys. Rev. **D81**, 092005, (2010).
- [60] Y. Nakajima *et al.*, Phys. Rev. **D83**, 012005, (2011).
- [61] J. S. O'Connell *et al.*, Phys. Rev. **C35**, 1063, (1987).